38

AN INVESTIGATION OF WING-BODY INTERFERENCE EFFECTS AT SUPERSONIC AND HYPERSONIC SPEEDS

PETER G. WILBY

The Aeronautical Research Institute of Sweden

ABSTRACT

A theoretical method for calculating second-order supersonic wing-body interference pressures is reviewed. Experimentally measured pressures on wings attached to cone-cylinder bodies are presented for Mach numbers of 3, 4, and 7, and the results compared with theoretical pressures which include second-order interference effects. It is seen that these effects appear at $M = 3$, become important at $M = 4$ and are large at $M = 7$. The interference theory gives very good results at Mach numbers of 4 and 7. The flow field round a blunt-nosed body is measured, prior to a study of the effect, on the pressure on a wing situated in this flow field, due to the entropy gradient generated by the body. A measured distribution over the wing is given, and compared with theoretical pressures which include contributions due to entropy gradient. The entropy gradient effect is found to be appreciable but not fully accounted for by the theory.

INTRODUCTION

Before the lift on the wing of a wing-body combination can be calculated with a reasonable degree of accuracy for high Mach number flight, various interference problems must be considered. First-order interference effects have been the subject of several papers which amply cover the problem, so this particular aspect can be considered solved and not requiring further attention. However, as Mach number increases, second-order interference effects become important. Also, with blunt-nosed bodies the flow over the wing is highly nonuniform and the influence of this nonuniformity on wing pressures may be important. In order to concentrate on the second-order problem, all wing-body combinations considered in this paper have nonlifting bodies. This means that the influence of first-order interference over the wing is restricted to the area between the wing root and the Mach line emanating from the leading edge of the wing-body

juncture. This region is small at high Mach numbers, and it is the remaining major part of the wing that will be considered here. Second-order wing-body interference will be considered first and experimental results will be compared with values calculated from the theory due to Landahl and Beane.[1] Then, the non-uniform flow about a blunt body at high Mach number will be considered with regard to the effect on the wing pressure of the entropy gradient existing in the flow. All results are for wings with sharp leading edges.

SECOND-ORDER WING-BODY INTERFERENCE

For the region on a wing outside the area of first-order interference influence, first-order theory gives the result that the velocity potential Φ is the sum of the potentials Φ_w and Φ_B due to the wing alone and the body alone respectively. However, as Mach number increases the second-order potential becomes important and Landahl and Beane show that the solution for the second-order potential ϕ includes an interference term due to cross products of wing and body first-order potentials, which occur in the linear differential equation for ϕ. Thus, Φ can be written as

$$\Phi = \Phi_W + \Phi_B + \phi_i \tag{1}$$

where ϕ_i is the interference part. Considering the expression for pressure coefficient,

$$C_P = -2\Phi_x + \beta^2\Phi_x^2 - \Phi_y^2 - \Phi_z^2 \tag{2}$$

where $\Phi = \varphi + \phi$ is the full velocity potential, it is seen that the term $\beta^2\Phi_x^2$ becomes appreciable at high Mach numbers. This term produces cross products

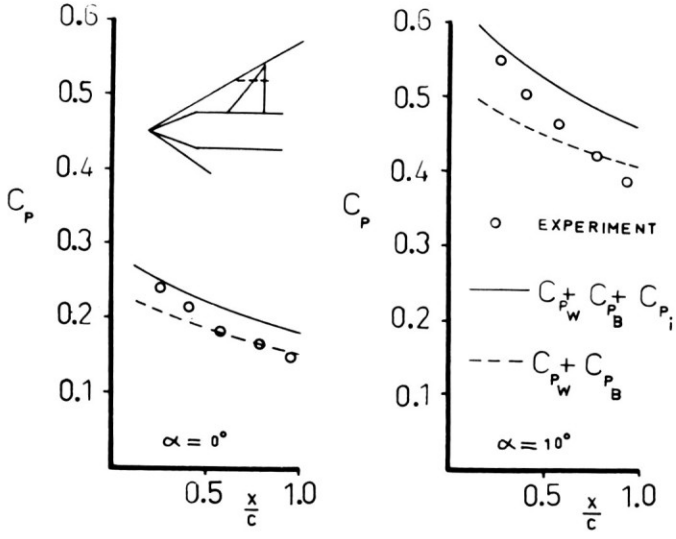

Fig. 1. Chordwise pressure distribution at $M = 3$.

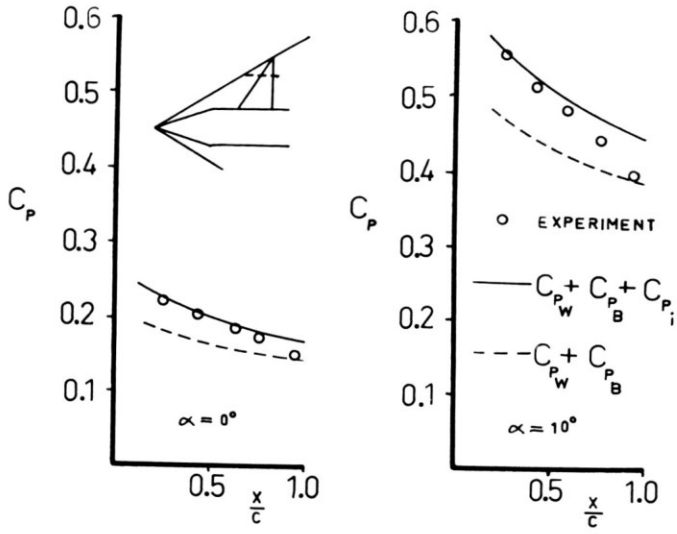

Fig. 2. Chordwise pressure distribution at $M = 4$.

of wing and body potentials, and, together with the terms due to ϕ_1, add up to give the interference pressure coefficient C_{P_i} when C_P is expressed as,

$$C_P = C_{P_W} + C_{P_B} + C_{P_i} \tag{3}$$

Landahl and Beane give the simplified result that

$$C_{P_i} = M^2(\gamma + 1)\varphi_{B_x}\,\varphi_{W_x} \tag{4}$$

which, on using the linearized piston theory approximation

$$\varphi_{W_x} = -\frac{1}{M}\,w \tag{5}$$

becomes

$$C_{P_i} = -M(\gamma + 1)\varphi_{B_x}{}^{w} \tag{6}$$

where w is the upwash on the wing surface. In Eq. (1) theoretical values for C_P which include interference effects are compared with results obtained from wind-tunnel tests at Mach numbers of 3 and 4 on wing-body models with wings at zero incidence. Theory and experiment have been compared, Eq. (2), at the same Mach numbers, but with wings at incidences in the range 0° to 10°. In the theoretical calculations, boundary-layer displacement thickness was accounted for in the values of C_{P_W}, and in order to find C_{P_i}, the approximation

$$\varphi_{B_x} = -\frac{1}{2}\,C_{P_B} \tag{7}$$

was used. Typical results for the chordwise pressure distributions are shown in Figs. 1 and 2 for Mach numbers of 2 and 4 respectively. In these cases the wings

were of triangular planform and had maximum thickness at the trailing edge, the bodies being of cone-cylinder form. Due to the position of the wings in the body fields, the largest interference effects were on the outer part of the wings. The spanwise positions of the chordwise pressure distributions are indicated in the figures. It is seen that at $M = 3$ the experimental results lie more or less between the theoretical results which include and exclude the interference part. However, at $M = 4$ the theoretical results including interference agree well with experiment, except near the trailing edge, where there is probably some pressure "leakage" from the trailing edge through the boundary layer. It is indicated in Eq. (2) that the interference theory is most accurate at higher Mach numbers and for lower sweepback angles of the wing, due to simplifying assumptions made in the theory. More recently, wind-tunnel tests have been performed on a model at $M = 7.3$ in the FFA hypersonic tunnel. At this high Mach number, Eq. (7) becomes rather approximate, but can be improved upon by a more accurate form. From Eq. (2) it can be seen that a close approximation to C_{P_B} is given by

$$C_{P_B} = -2\varphi_{B_x} + \beta^2 \varphi_{B_x}{}^2$$

This equation then gives

$$\varphi_{B_x} = \frac{1}{\beta^2}\left[1 - (1 + \beta^2 C_{P_B})^{1/2}\right] \tag{8}$$

which of course reduces to Eq. (7) when $\beta^2 C_{P_B} \ll 1$. Eq. (8) also becomes a rather rough approximation at high Mach number and high incidence, as it comes from combining the two approximate relations

$$\varphi_{W_x} = -\tfrac{1}{2} C_{P_W} \tag{9}$$

and

$$C_{P_W} = \frac{2w}{M} \tag{10}$$

The second of these comes from the full piston theory result

$$C_{P_W} = \frac{2w}{M} + \frac{\gamma + 1}{2} w^2 + \frac{\gamma + 1}{6} M w^3 \tag{11}$$

Obviously for a wing at high incidence and high Mach number, the second and third terms in Eq. (11) are both very important on the pressure surface of the wing where w is large. Thus, whereas Eq. (5) is a valid approximation at Mach numbers of 3 and 4, it is no longer so at $M = 7$, especially for a wing at incidence. Eq. (9) can be replaced by a more accurate form as was done in the body field case, giving

$$\varphi_{W_x} = \frac{1}{\beta^2}\left[1 - (1 + \beta^2 C_{P_W})^{1/2}\right] \tag{12}$$

where C_{P_W} can be calculated from Eq. (11). In fact, C_{P_W} was calculated by Bertram's method[3] which is a method of two-dimensional wings and includes an approximate allowance for boundary-layer displacement thickness. Pressure coefficients calculated by this method are compared in Figs. 3 and 4 with experimental values. Also shown are theoretical values obtained from Eq. (11) with w adjusted to include boundary-layer effects calculated according to Bertram. Bertram's method is seen to give good results, whereas piston theory fails at high incidence (which is of course to be expected). Bertram's method was thus used for all calculations of C_{P_W}, and C_{P_i} was calculated from Eqs. (4), (8), and (12). Pressure coefficients calculated in this way are shown in Fig. 3 for an outer section on the pressure surface of the wing at 10° incidence. The results are compared with experiment and also with theory, using Eqs. (6) and (7) for C_{P_i}, and are seen to agree well with experiment. It is also shown that the more accurate expressions for φ_{W_x} and φ_{B_x} give better results. It should however be noted that the errors which arise through the use of Eqs. (5) and (7) tend to cancel each other to a certain extent as Eq. (5) underestimates φ_{W_x} and Eq. (7) overestimates φ_{B_x}. Again, interference was found to be greatest over the outer part of the wing and pressure distributions along two chordwise sections are given in Fig. 4 for various angles of incidence. As interference pressures on the upper surface of a wing at incidence are very small, the interference pressure on the lower surface can be taken to be the lifting pressure due to interference. The importance of interference effects and the accuracy with which they can be predicted is evident.

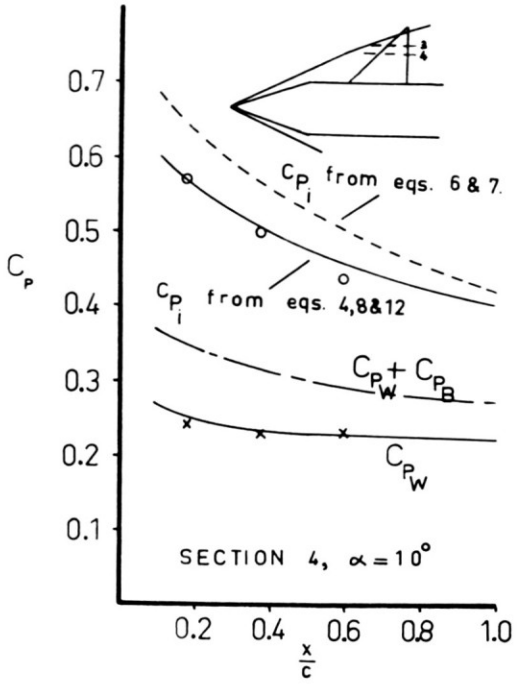

Fig. 3. Chordwise pressure distribution at $M = 7.3$.

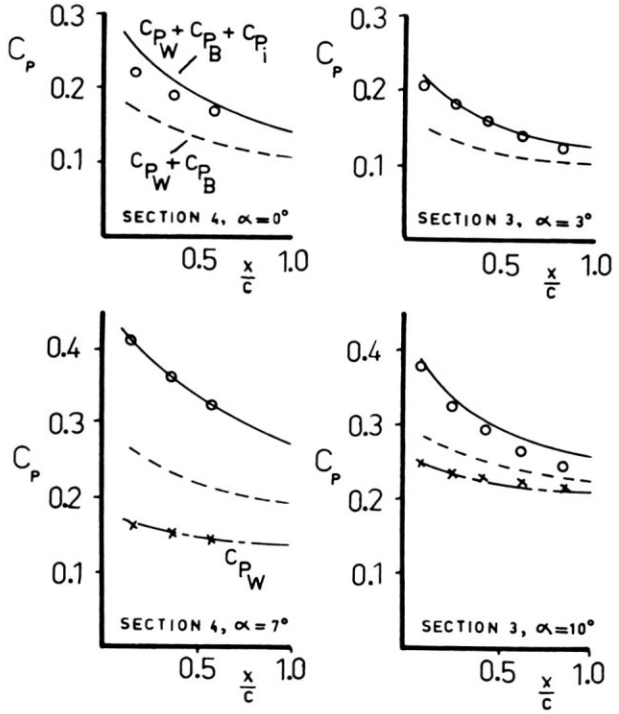

Fig. 4. Chordwise pressure distributions at $M = 7.3$.

THE FLOW ABOUT A BLUNT-NOSED BODY OF REVOLUTION AT HYPERSONIC SPEED

For a wing-body combination with a blunt-nosed body, traveling at high Mach number, there will be an entropy gradient in the radial direction (with respect to the body) due to the large curvature of the body shock. Thus, for a radially mounted wing there will be a spanwise entropy gradient along the wing. If the entropy gradient effects are large, it may be that the methods discussed in the first part of this paper will no longer be sufficient for an accurate determination of the wing pressure. With this in mind, an investigation was undertaken to discover the magnitude of entropy gradient effects. This model chosen for the investigation was a hemisphere-cylinder body with a radially mounted wing of wedge section. Wind-tunnel tests were made in the FFA hypersonic tunnel at a Mach number of 7.3. In order to calculate the separate wing- and body-field pressures, so as to be able to find the entropy gradient effect, it was necessary to study the body-field flow. This was done experimentally, and the static pressure and Mach number distributions were calculated from pitot tube measurements and the body shock shape. As the determination of the body field is thought to be of interest, a few details of the method employed and the results obtained are given here. The whole of the body-field flow (except of course the region at the nose) is supersonic, so a shock wave forms ahead of the pitot

tube which then measures the stagnation pressure behind this shock. The Mach number can be found, provided the stagnation pressure ahead of the pitot shock is known. To find the stagnation pressure ahead of the pitot shock, it is necessary to know the point at which the streamline, along which the pitot tube is positioned, crosses the body shock. The stagnation pressure can then be calculated from the oblique shock relations, taking the shock slope from a schlieren photograph. Thus the problem now is to find a relation between the radial positions r_j of the pitot tube, and r_{s_j} of the point of the body shock at which the streamline crosses the shock, where r is measured from the body axis. Remembering that there can be no flow across streamlines, the axial continuity of mass flow gives the following integral relation:

$$(r_{s_j})^2 = 2 \int_{r_b}^{r_i} \frac{\rho_2 U_2}{\rho_\infty U_\infty} r \, dr \tag{13}$$

where r_b is the body radius and the subscripts 2 and ∞ denote conditions just ahead of the pitot shock, and free stream respectively. The ratio of density-velocity products can be written as

$$\frac{\rho_2 U_2}{\rho_\infty U_\infty} = \frac{M_2}{M_\infty} \left(\frac{1 + \frac{\gamma - 1}{2} M_\infty^2}{1 + \frac{\gamma - 1}{2} M_2^2} \right)^{\frac{1+\gamma}{2(\gamma-1)}} \left(\frac{p_{o_1}}{p_o} \right)^{\frac{1+\gamma}{2\gamma}} \left(\frac{p}{p_1} \right)^{\frac{1}{2\gamma}} \left(\frac{\rho_1}{\rho} \right)^{\frac{1}{2}} \tag{14}$$

where the subscript 1 denotes conditions immediately behind the body shock. The last three terms in Eq. (14) can be found from oblique shock relations provided r_{s_j} is known. M_2 can be calculated from the measured stagnation pressure and r_{s_j}. Obviously the only way to calculate M_2 and p_2 is a step by step iterative process along a radial line, starting at the body surface. Starting at a point close to the body surface, r_{s_1} is estimated and from this a value of p_{o_1}, which is also the stagnation pressure ahead of the pitot shock, is found. Using this value of p_{o_1} together with the measured stagnation pressure M_2 can be calculated. The static pressure p_2 can then be obtained from M_2 and p_{o_1}. Now, the integrand in Eq. (13) can be evaluated, and assuming the static pressure to be constant in the region close to the body, the integrand can also be evaluated at the body surface "b" as obviously $r_{s_b} = 0$. A new value for r_{s_1} can now be found by graphical integration according to Eq. (13), the calculations being repeated until the values of r_{s_1} converge. The final values of M_2 and p_2 can be obtained before moving on to the next point. The final point of evaluation on the section is the intersection "n" with the body shock. Here the integrand can be evaluated directly from oblique shock relations and then the graphical integration, using all the previously calculated integrands, should give a value of r_{s_n} equal to r_n. This provides a useful check on the calculations. Seiff and Whiting[4] give a method for calculating the downstream flow about a blunt body of revolution with calculations based on bow shock shape and blast-wave theory. They assume that the radial pressure distribution between the

body and the shock can be obtained from blast-wave theory by using the similarity relation

$$\frac{p(r) - p_b}{p_n - p_b} = \left[\frac{p(r) - p_b}{p_n - p_b}\right]_{\text{B.W.}} \tag{15}$$

where p_n is the pressure at the shock wave on the section of evaluation. This method, however, can only be used well downstream of the body nose, whereas the technique described above can be employed much nearer the nose, the insensitivity of the pitot tube to moderate flow inclinations being a useful property. Radial distributions of pressure coefficient are shown in Fig. 5 for various positions "x" downstream of the nose. In the figure, x is nondimensionalized with respect to the body diameter d. Also shown are the pressure coefficients given by blast-wave theory. It is seen that there is considerable difference between the results, but agreement improves as x increases. However, it should be pointed out that the pitot method results have not been corrected for wind-tunnel flow nonuniformities. Such corrections would probably not have been very large, but anyway they were not necessary in the investigation of the pressure distribution over a wing placed in the body field. All that was required was the net body field, its composition being irrelevant. Also, the body used was not a full body of revolution as almost half was removed (see Fig. 6) for tunnel

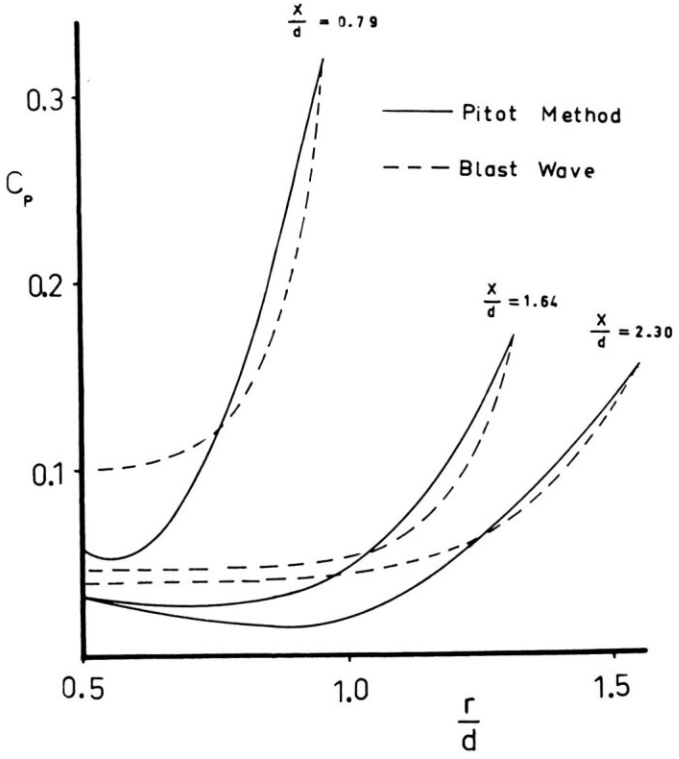

Fig. 5. Radial pressure distributions for body at $M = 7.3$.

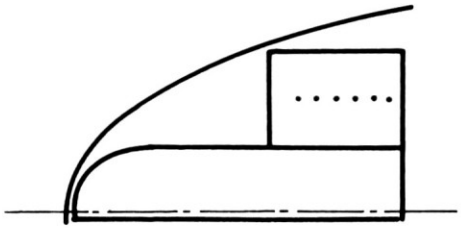

Fig. 6. Model configuration for entropy gradient test.

blockage considerations. This resulted in the shock shape close to the stagnation point being slightly different from that for a full body of revolution. The flow close to the body was thus slightly different from that around a full body.

Having determined the body field, a position was chosen in which to mount a straight wing of wedge section on which could be measured a chordwise pressure distribution. Knowledge of the body field was also required to provide information necessary for the attempt to calculate theoretically the effect of the entropy gradient. The aim of the theoretical approach was to find an expression for the contribution C_{P_s} to the total pressure coefficient, which was due to the entropy gradient. It would then be possible to express the full pressure coefficient as

$$C_P = C_{P_W} + C_{P_B} + C_{P_i} + C_{P_s}$$

where C_{P_W}, C_{P_B} and C_{P_i} can be calculated by the method mentioned previously.

THE EFFECT OF A SPANWISE ENTROPY GRADIENT ON THE PRESSURE ON A WING

The case of a thin infinite wing in supersonic flow with a spanwise entropy gradient has been studied theoretically.[5] An entropy gradient is assumed to be introduced in the y-direction across a uniform parallel flow of velocity U_0, resulting in a parallel flow of velocity $U_0 + u_1(y)$. The flow over the wing situated in the nonuniform flow with its span along the y-direction is then considered. Denoting the perturbation velocity components over the wing by u, v, and w in the x, y, and z directions respectively, where the direction of the free-stream flow is in the positive x-direction, Crocco's equation is shown to produce the following three equations:

$$v\left(\frac{\partial v}{\partial x} - \frac{\partial u}{\partial y}\right) - w\left(\frac{\partial u}{\partial z} - \frac{\partial w}{\partial x}\right) = 0 \tag{16}$$

$$w\left(\frac{\partial w}{\partial y} - \frac{\partial v}{\partial z}\right) - (U_0 + u_1 + u)\left(\frac{\partial v}{\partial x} - \frac{\partial u}{\partial y}\right) - u\frac{du}{dy}1 \tag{17}$$

$$(U_0 + u_1 + u)\left(\frac{\partial u}{\partial z} - \frac{\partial w}{\partial x}\right) - v\left(\frac{\partial w}{\partial y} - \frac{\partial v}{\partial z}\right) = -\frac{du}{dy}1\int_0^x \frac{\partial v}{\partial z}\,dx \tag{18}$$

It is assumed that u and w will differ only slightly from their values in the two-dimensional case, and that it is still possible to write

$$\frac{\partial u}{\partial z} - \frac{\partial w}{\partial x} = 0 \tag{19}$$

Then, u and w are expressed as differentials of a potential function Φ which is the normal two-dimensional potential plus an extra second-order term ϕ_s due to the entropy gradient. Equations (16) to (19) are then solved for v, which is expressed in terms of the first-order solution φ to Φ, and the change in pressure coefficient C_{P_s} is given in terms of v and ϕ_s. The expression obtained for v can be written

$$\frac{v}{U_0 + u_1} = -\lambda(\beta^2\varphi_x + 1) + \beta^2 z\varphi_{xx}\frac{d\beta}{dy} \tag{20}$$

where $\lambda = (1/U_0 + u_1)\ (du/dy)\ 1$ which is considered constant.

In order to calculate $d\beta/dy$ in the flow ahead of the wing, it is assumed in Ref. 5 that

$$\rho(U_0 + u_1) = \text{Const.}$$

This could be true for a two-dimensional case provided the streamline spacing was the same before and after the entropy discontinuity. However, the case of an entropy discontinuity due to the shock produced by a body of rotation is not quite so simple, as the radial distance of the streamlines from the axis of symmetry must be considered, requiring a continuity equation of the type given in Eq. (13). It was found in the body-field investigation that the gradient of β was

$$\frac{d\beta}{dy} = 0.15\beta$$

Calculations showed that ϕ_s was, in fact, negligible so that the pressure coefficient part due to the entropy gradient was simply

$$C_{P_s} = -\left(\frac{v}{U_0}\right)^2$$

i.e.,

$$C_{P_s} = -\left(\frac{v}{U_0 + u_1}\right)^2\left(\frac{U_0 + u_1}{U_0}\right)^2$$

which can be written approximately as

$$C_{P_s} = -\left(\frac{v}{U_0 + u_1}\right)^2\left(1 + \varphi_{B_x}\right)^2$$

The entropy profile across the flow was calculated from the shape of the body shock and the streamline pattern round the body. Then, the parameter λ was found from the slope of this profile using the relation

$$\lambda = -\frac{1}{M^2 R}\frac{dS}{dy}$$

where M is the local Mach number and R the gas constant. The variation of λ with y is shown in Fig. 7 where it is seen to be constant over a large portion of the wing span. C_{P_s} was calculated according to Eqs. (20) and (21), and the full theoretical pressure coefficient is shown in Fig. 8, where it is compared with the experimental values. The experimental values are seen to lie well below those given by theory excluding entropy gradient effects. Even when these effects are

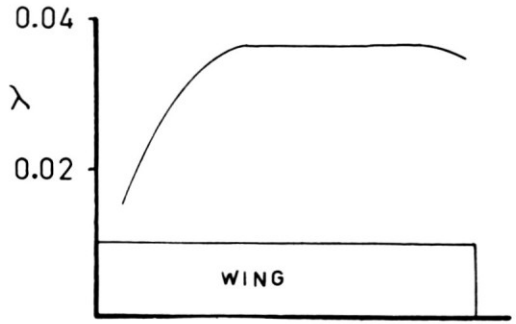

Fig. 7. Spanwise distribution of entropy gradient parameter λ.

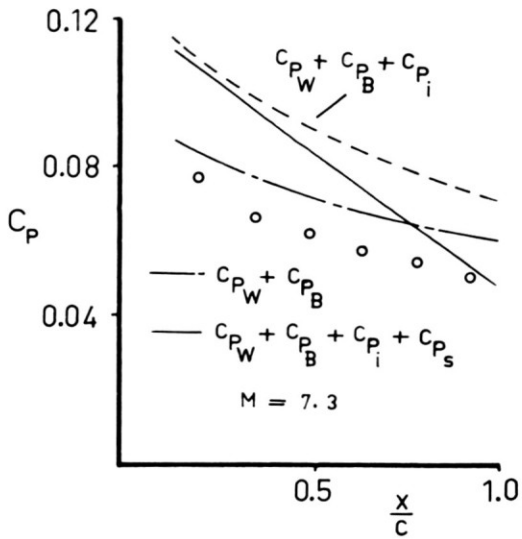

Fig. 8. Chordwise pressure distribution for entropy gradient case.

included in the theory there is still a large difference between theory and experiment. The method for obtaining C_{P_W} and C_{P_i} has been shown to be fairly accurate and the procedure for finding C_{P_B} should give good results. So, the difference between experimental results and the theory without entropy gradient effects can be taken as a fair measure of the true entropy gradient effects. This shows the theoretical determination of C_{P_s} to be rather inadequate and that an improved theory is required. Since this difference between theory and experiment arises it is probable that the assumption that the velocities u and v over the wing have almost their two-dimensional values is not quite true.

CONCLUSIONS

Second-order wing-body interference begins to affect the wing pressures at about $M = 3$ and at $M = 4$ it can be important, especially for wings at incidence. At a Mach number of 7 the interference pressure can be very large. The second-order interference theory gives very good results at Mach numbers of 4 and 7, the accuracy of the results at $M = 7$ indicating that the theory is valid at even higher Mach numbers. In the case of a blunt-nosed body, when an entropy gradient is generated across the flow field in which the wing is situated, there appears to be a considerable contribution to the wing pressure due to the entropy gradient. This contribution is not satisfactorily accounted for by the theory used, and an improved theory is required before an accurate determination of the total wing pressure can be made.

ACKNOWLEDGMENTS

The investigation was sponsored by the ARDC through its European Office under Contract No. AF 61 (052)–75.

The author is greatly indebted to Dr. G. Drougge for his valuable advice and assistance.

REFERENCES

1. Landahl, M., G. Drougge, and B. Beane, "Theoretical and Experimental Investigation of Second-order Supersonic Wing-body Interference," *J. Aerospace Sci.*, September 1960.
2. Wilby, P. G., "An Experimental and Theoretical Investigation of Second-order Supersonic Wing-body Interference for a Nonlifting Body with Wings at Incidence," *FFA Report 87*, October 1960.
3. Bertram, M. H., "An Approximate Method for Determining the Displacement Effects and Viscous Drag of Laminar Boundary Layers in Two-dimensional Hypersonic Flow, *NACA TN 2773*, September 1952.
4. Seiff, A., and E. F. Whiting, "Calculation of the Flow Fields from Bow-wave Profiles for the Downstream Region of Blunt-nosed Circular Cylinders in Axial Hypersonic Flight," *NASA TN D–1147*, 1961.
5. Wilby, P. G., "Second-order Theory for a Thin Wing in Supersonic Flow with a Weak Spanwise Entropy Gradient," *FFA Report 88*, June 1961.